### Title

Potential Role of Stabilized Criegee Radicals in Sulfuric Acid Production in a High Biogenic VOC Environment




### Journal

Environmental Science and Technology, 49(6)

### ISSN

0013-936X



### Authors

Kim, Saewung
Guenther, Alex
Lefer, Barry
et al.



### Publication Date

2015-03-17

### DOI

10.1021/es505793t

Environmental Science & Technology

Article

pubs.acs.org/est

# Potential Role of Stabilized Criegee Radicals in Sulfuric Acid Production in a High Biogenic VOC Environment

Saewung Kim,*[,†] Alex Guenther,[‡,§] Barry Lefer,[∥] James Flynn,[∥] Robert Griffin,[⊥] Andrew P. Rutter,[⊥,#] Longwen Gong,[⊥,▽] and Basak Karakurt Cevik[⊥]

[†]Department of Earth System Science, University of California—Irvine, Irvine, California 92697, United States

[‡]Atmospheric Sciences and Global Change Division, Pacific Northwest National Laboratory, Richland, Washington 99354, United States

[§]Department of Civil and Environmental Engineering, Washington State University, Pullman, Washington 99164, United States

[∥]Department of Earth and Atmospheric Sciences, University of Houston, Houston, Texas 77004, United States

[⊥]Department of Civil and Environmental Engineering, Rice University, Houston, Texas 77005, United States

[#]S.C. Johnson & Son, Inc., Racine, Wisconsin 53403, United States

[▽]California Air Resource Board, Monitoring and Laboratory Division, Sacramento California 95811, United States



**ABSTRACT:** We present field observations made in June 2011 downwind of Dallas−Fort Worth, TX, and evaluate the role of stabilized Criegee radicals (sCIs) in gaseous sulfuric acid ($H_2SO_4$) production. Zero-dimensional model calculations show that sCI from biogenic volatile organic compounds composed the majority of the sCIs. The main uncertainty associated with an evaluation of $H_2SO_4$ production from the sCI reaction channel is the lack of experimentally determined reaction rates for sCIs formed from isoprene ozonolysis with $SO_2$ along with systematic discrepancies in experimentally derived reaction rates between other sCIs and $SO_2$ and water vapor. In general, the maximum of $H_2SO_4$ production from the sCI channel is found in the late afternoon as ozone increases toward the late afternoon. The sCI channel, however, contributes minor $H_2SO_4$ production compared with the conventional OH channel in the mid-day. Finally, the production and the loss rates of $H_2SO_4$ are compared. The application of the recommended mass accommodation coefficient causes significant overestimation of $H_2SO_4$ loss rates compared with $H_2SO_4$ production rates. However, the application of a lower experimental value for the mass accommodation coefficient provides good agreement between the loss and production rates of $H_2SO_4$. The results suggest that the recommended coefficient for the $H_2O$ surface may not be suitable for this relatively dry environment.

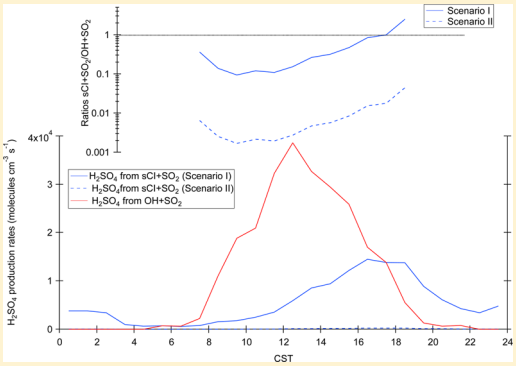


## INTRODUCTION

Most sulfur compounds emitted to the atmosphere are in a reduced form (e.g., sulfur dioxide, $SO_2$ (IV)). Atmospheric gas-phase oxidation processes sulfur throughout the troposphere and the stratosphere and transforms these emitted sulfur compounds into the most oxidized form of gas-phase sulfuric acid ($H_2SO_4$), unless heterogeneous uptake transforms the sulfur into condensed-phase forms. The discussion in this paper will focus exclusively on gas-phase $H_2SO_4$ formation from gas-phase $SO_2$ oxidation. Although sulfur compounds contribute a relatively minor fraction of the chemical composition of the troposphere,[1] the critical role of $H_2SO_4$ in determining acidity in precipitation[2] and forming particles that influence regional and global climate has been highlighted.[3−5] Anthropogenic sulfur emission in the form of $SO_2$ is currently estimated to dominate global sulfur emissions, followed by oceanic dimethylsulfide ($CH_3SCH_3$).[6] The gas-phase atmospheric oxidation processes of $SO_2$ were thought previously to be driven mostly by hydroxyl radical (OH), as shown in R1−R3.[7]

$$SO_2 + OH + M \rightarrow HSO_3 + M \quad (R1)$$

$$HSO_3 + O_2 \rightarrow SO_3 + HO_2 \quad (R2)$$

$$SO_3 + H_2O \rightarrow H_2SO_4 \quad (R3)$$

The potential role of stabilized Criegee biradicals (sCIs)[8] in $SO_2$ oxidation has been discussed since the 1970s. Cox and Penkett[9] reported significant $SO_3$ formation rates from chamber experiments with various alkene compounds, ozone ($O_3$), and $SO_2$. They speculated sCIs prompted $SO_2$ oxidation because the reaction between $SO_2$ and $O_3$ is insignificant under atmospheric conditions. Calvert and Stockwell[2] presented comprehensive zero-dimensional model calculation results examining atmospheric acid formation under various physical and chemical

Received: November 29, 2014
Revised: February 19, 2015
Accepted: February 20, 2015
Published: February 20, 2015




DOI: 10.1021/es505793t
Environ. Sci. Technol. 2015, 49, 3383−3391

Table 1. Summary of Field Deployed Instrumentation Referred in This Study during DFW-2011

| species/parameter | measurement technique |
|---|---|
| CO | Thermo Electron Corp. 48C Trace Level CO Analyzer (Gas Filter Correlation) |
| $SO_2$ | Thermo Electron Corp. 43C Trace Level $SO_2$ Analyzer (Pulsed Fluorescence) |
| $NO_x$ | Thermo Electron Corp. 42C Trace Level NO—$NO_2$—$NO_x$ Analyzer (Chemiluminescence) |
| $NO_y$ | Thermo Electron Corp. 42C—Y $NO_y$ Analyzer (Molybdenum Converter) |
| VOCs | PTR-ToF-MS (Ionicon Analytik) and GC-FID |
| OH and $H_2SO_4$ | Chemical Ionization Mass Spectrometer |
| particle mobility-based size distribution | Scanning Electrical Mobility Spectrometer Model 2002 (Brechtel Manufacturing) |
| temperature, relative humidity | Cambell Scientific HMP45C-L temperature and relative humidity probe |

conditions. The study suggested that the reaction between sCIs (here shown as $CH_2OO$) and $SO_2$ could account for up to 50% of the atmospheric $H_2SO_4$ production in dry conditions (RH = 10% at 25 °C) but becomes insignificant as conditions become more humid because the reaction between $SO_2$ and sCI (R4) competes with the reaction between water vapor and sCI (R5).

$$CH_2OO + SO_2 \rightarrow HCHO + SO_3 \quad (R4)$$

$$CH_2OO + H_2O \rightarrow HCHO + H_2O_2 \quad (R5a)$$

$$CH_2OO + H_2O \rightarrow HCOOH + H_2O \quad (R5b)$$

Hatakeyama et al.[10] presented $H_2SO_4$ yields from $SO_2$ and sCI from different alkene and dialkene ozonolysis experiments for a wide range of pressures in a reaction vessel. They reported that $H_2SO_4$ yields are highly pressure and chemical species dependent. Further, Johnson et al.[11] presented an experimentally derived rate constant for R4 ($k_4$ =$4.9 \times 10^{-15}$ $cm^3$ $molecule^{-1}$ $s^{-1}$ as an upper limit) determined by tracking reaction precursors and products using a gas chromatograph (GC)-flame ionization detection (FID) system. This is significantly smaller than the reaction rate constant of R1 ($1.3 \times 10^{-12}$ $cm^3$ $molecule^{-1}$ $s^{-1}$ at 298 K and 1 atm). Therefore, the research community concluded that contributions of R4 to atmospheric $H_2SO_4$ production should be negligible for tropospheric conditions. As analytical techniques became available for the direct quantification of sCI, recent studies[12,13] reevaluated the rate constants for R4 based on observations that indicate these rate constants are significantly larger than previously thought ($3.9 \times 10^{-11}$ $cm^3$ $s^{-1}$, $k_{Welz}$). Taatjes et al.[14] presented experimental observations of reactivity of the $CH_3CHOO$. The results also consistently indicate faster reaction rates of $SO_2$ with *anti*-$CH_3CHOO$ ($6.7 \times 10^{-11}$ $cm^3$ $s^{-1}$) and *syn*-$CH_3CHOO$ ($2.4\times 10^{-11}$ $cm^3$ $s^{-1}$) that are close to $k_{Welz}$. Mauldin et al.[15] presented rate constants of $SO_2$ reaction with sCI formed from oxidation of monoterpenes ($C_{10}H_{16}$; $\alpha$-pinene and limonene) as $\sim 6 \times 10^{-13}$ $cm^3$ $s^{-1}$ ($k_{Mauldin}$) by directly quantifying $H_2SO_4$ using a chemical ionization mass spectrometer (CIMS). A follow up study using an identical experimental configuration[16] to study sCIs from isoprene and monoterpene ozonolysis confirmed the results of Mauldin et al.[15] Currently, it is not clear whether the significant difference between $k_{Welz}$ and $k_{Mauldin}$ results from the different molecular structures or systematic differences in experimental configurations. It is notable that Carlsson et al.[17] presented an experimentally determined reaction rate of $SO_2$ with sCIs from $\beta$-pinene that is close to $k_{Welz}$. However, this study did not directly quantify either sCIs or $H_2SO_4$ but interpreted reaction rates by observing oxidation products of $\beta$-pinene using infrared absorption spectra. In summary, despite uncertainty in the rate constants remaining large, recent experimental findings consistently indicate that the sCI reaction channel in $H_2SO_4$ production previously has been underestimated.

Implications of the proposed faster reaction rates have been investigated from local to global scales. A one-dimensional modeling study[18] illustrated that using the newly reported rate constants results in $H_2SO_4$ levels that are 33−46% higher inside a forest canopy in a clean boreal forest with high monoterpene levels. In contrast, a global modeling study[19] observed only a small increase (4%) of $H_2SO_4$ by applying the faster rate constants on the global scale. More recently, a laboratory study[13] showed that the reaction rate of R5 is much lower ($5.4 \times 10^{-18}$ $cm^3$ $s^{-1}$) than what was previously reported[12] ($4 \times 10^{-15}$ $cm^3$ $s^{-1}$). Therefore, the study argued that the previous evaluations on the impact of the $CH_2OO$ + $SO_2$ reaction in $H_2SO_4$ formation should be understood as a lower limit since the importance of R5 competition with R4 for sCI may be overestimated. Discussion on the importance of the sCI reaction channel in aerosol sulfate formation using regional chemical transport models also have been presented,[20,21] but our discussion is limited to gas-phase chemistry.

In June 2011, comprehensive observations including carbon monoxide (CO), nitrogen oxides ($NO_x$ = NO + $NO_2$), total reactive nitrogen ($NO_y$), $SO_2$, $O_3$, volatile organic compounds (VOCs), OH, $H_2SO_4$, and aerosol surface area were conducted at the Eagle Mountain Lake monitoring site in Tarrant County, TX, northwest of the metropolitan Dallas−Fort Worth (DFW) area. This site is influenced mostly by urban pollution outflow, but significant levels of biogenic VOCs (BVOCs) were detected frequently due to the surrounding rural area. The data set is presented to assess quantitatively the role of sCIs in $H_2SO_4$ production. A zero-dimensional model is employed to estimate sCI concentrations formed from VOC precursors to evaluate $H_2SO_4$ production rates from the OH reaction channel (R1) and the sCI reaction channel (R4). Finally, we examine $H_2SO_4$ uptake to aerosol surface to compare with $H_2SO_4$ production rates, as aerosol uptake is known to be the dominant $H_2SO_4$ sink.[22] These analyses provide an opportunity to comprehensively assess our current understanding of tropospheric $H_2SO_4$.

## METHODS

**Observations.** Observations were conducted in June of 2011 at the Eagle Mountain Lake monitoring site. The inlets for gas phase analysis (CO, $NO_x$, $NO_y$, $SO_2$, $O_3$, and VOCs) were installed on top of a walk-up tower (~10 m from the ground) using perfluoroalkoxy Teflon tubing (1/4″ OD). Analytical techniques for gas, particle, and meteorological parameters presented in this study are summarized in Table 1. Online aerosol measurements were conducted using an inlet separate from that for the gas-phase instrumentation. It consisted of stainless steel tubing of 3/8″ OD. The end of the inlet was approximately 3 m above ground level and included a $PM_{2.5}$ cyclone to ensure that only fine PM was collected. Aerosol surface area distributions were calculated from measured





DOI: 10.1021/es505793t
Environ. Sci. Technol. 2015, 49, 3383−3391

distributions of the mobility aerodynamic diameter determined by a Brechtel Manufacturing, Inc., Scanning Electrical Mobility Spectrometer Model 2002. VOC observations were conducted using an IONICON Analytik GmbH proton transfer reaction-time-of-flight-mass spectrometer (PTR-ToF-MS 8000).[23] This technique uses protonated water ($H_3O^+$) as the reagent ion and can quantify a wide range of VOCs that have higher proton affinity than $H_2O$[24](691 kJ $mol^{-1}$), including many of the important biogenic and anthropogenic VOCs. A MATLAB (MathWorks) script was used to calculate 1 min average data from raw data files containing 1 s average spectra.[25] Weekly multipoint calibration was conducted with a multicompound calibration standard (methanol, acetonitrile, acetaldehyde, acetone, methyl vinyl ketone (MVK), limonene, 2-methyl-3-butene-2-ol, benzene, and methyl ethyl ketone), prepared by the NOAA Chemical Sciences Division in Boulder, CO. The background signal was assessed with VOC-scrubbed ambient air utilizing a heated Pt-wool catalytic converter (400 °C).[26] The estimated analytical uncertainty is 15% (2 $\sigma$), and the lower limit of detection is ~20 ppt for a 1 min average (2 $\sigma$). Because the PTR-ToF-MS technique used does not provide quantification of alkane and light alkene compounds, a publicly available AutoGC data set collected at the observational site was used for this study (http://www.tceq state.tx.us/cgi-bin/compliance/monops/site_photo.pl?cams=75). Texas Commission on Environmental Quality (TCEQ) maintains operation and reporting of the VOC data under the EPA quality guidelines.

The $H_2SO_4$ and OH observations were conducted using a CIMS with an atmospheric pressure ionization system.[27] The nitrate ion system was used to ionize $H_2SO_4$. Atmospheric OH was first converted into $H_2{}^{34}SO_2$ by adding excess $^{34}SO_2$ in the sample flow. More detailed descriptions of the instrument are reported elsewhere.[28,29] Analytical uncertainties for OH and $H_2SO_4$ analysis are assessed to be 35% (3$\sigma$) including the statistical errors from the calibration procedures for the 1 min period. The assessed lower limit of detection for both OH and $H_2SO_4$ was $1 \times 10^5$ molecules $cm^{-3}$ (2$\sigma$).

**Zero-Dimensional Model.** The University of Washington Chemical Mechanism (UWCM; https://sites.google.com/site/wolfegm/models) v2.1[30] was used for sCI calculations. The chemical mechanisms of methane, ethane, propane, *n*-butane, *iso*-butane, *n*-pentane, iso-pentane, *n*-hexane, *n*-heptane, ethene, propene, 1-butene, *cis*-2-butene, benzene, toluene, butadiene, isoprene, $\alpha$-pinene, and $\beta$-pinene were extracted from Master Chemical Mechanism (MCM; http://mcm.leeds.ac.uk/MCM/) v3.2[31−33] for the UWCM model calculations on top of the embedded $HO_x$−$NO_x$ chemical mechanisms. Isoprene oxidation schemes were updated as described in Archibald et al.[34] The photolysis rates were calculated using the scheme presented in Saunder et al.[33] The sCI reaction channels[35] were incorporated explicitly in MCM v3.2, and the model calculations were conducted using the default rate constants (e.g., with CO, NO, $NO_2$, and $H_2O$), except the rates of sCIs with $SO_2$ as described in Table 2. In addition, R5a was updated as shown in Stone et al.[13] We constrained observed concentrations of CO, $NO_x$, $SO_2$, ozone, VOCs, OH, ambient temperature, and humidity to calculate seven sCIs (Table 2) so that we can evaluate $H_2SO_4$ formation rates from reactions between $SO_2$ and sCI. This model calculation scheme can be found in previous publications.[28,36] This zero-dimensional modeling approach has the advantage of being able to estimate short-lived radical species while avoiding uncertainty introduced by the processes associated with vertical and horizontal chemical transport and emissions by constraining relatively long-lived trace gas species. Therefore, this approach is used commonly by the radical observation community to examine whether current photochemical understanding explains observed radical levels.[28,29,36−38] We compared model predicted MVK + MACR (methacrolein) levels with the observations for the sensitivity test, which indicates acceptable agreement (within 40%). The results indicate that UWCM 2.1 reliably describes the complicated $HO_x$−$NO_x$−VOCs system.

**Table 2. Summary of Reaction Constants between sCI and $SO_2$ Applied for the $H_2SO_4$ Formation Potential Analysis[a]**

| | scenario I | scenario II |
|---|---|---|
| $CH_2OO$ | $k_{Welz}$ | $k_{Mauldin}$ |
| $CH_3CH$ | $k_{Welz}$ | $k_{Mauldin}$ |
| $C_2H_5CHOO$ | $k_{Welz}$ | $k_{Mauldin}$ |
| APINBOO[b] | $k_{Welz}$ | $k_{Mauldin}$ |
| MVKOO[c] | $k_{Welz}$ | $k_{Mauldin}$ |
| MACROO[c] | $k_{Welz}$ | $k_{Mauldin}$ |
| NOPINOO[d] | $k_{Welz}$ | $k_{Mauldin}$ |

[a] $k_{Welz}$ = $3.9 \times 10^{-11}$ $cm^3$ $s^{-1}$ and $k_{Mauldin}$ = $6 \times 10^{-13}$ $cm^3$ $s^{-1}$. [b] sCI from $\alpha$-pinene ozonloysis. [c] sCIs from isoprene ozonloysis. [d] sCI from $\beta$-pinene ozonloysis.

## RESULTS AND DISCUSSION

A global modeling study[19] concluded that $H_2SO_4$ production from sCIs was signficant only in high BVOC environments. To explore roles of sCIs in $H_2SO_4$ production, as shown in Figure 1, a five-day period (June 17th to June 21st, indicated as a green square) of enhanced BVOC influences was selected from the month-long study.

Observed trace gas diurnal variations used for zero-dimensional model constraints are presented in Figure 2. In general, criteria pollutants such as CO, $NO_2$, and $SO_2$ were observed at smaller mixing ratios during this five-day period, compared with the whole observational period (Figure 1). The observed NO level was typically more than a few hundred ppt, which can be considered as the high $NO_x$ regime for the peroxy radical chemistry perspective.[36] The diurnal variations of the observed VOCs are also summarized in Figure 2. Each chemical class such as alkanes, alkenes, aromatics, and BVOCs shows distinctive diurnal variations. BVOCs and alkanes especially indicate contrasting diurnal variations. These differences are caused by the complex interplay of emissions, photochemistry, and meteorological processes such as boundary layer height evolution and advection.

This is the first published OH observation in the DFW metropolitan area. However, field OH observations have been conducted in Houston, TX. The averaged midday OH concentrations from two Houston, TX field campaigns in the summer season were in the range of $1.5 \times 10^7$ to $2.0 \times 10^7$ molecules $cm^{-3}$,[38] which is much higher than the OH levels observed during this study. However, the afternoon $O_3$ levels observed during the Houston field campaigns (75 ppb) were much higher than the $O_3$ levels during this study. In general, the observed OH levels for this study are comparable with previously reported OH levels from other moderately polluted environments.[39] The observed daytime $H_2SO_4$ maximum was ~$7 \times 10^6$ molecules $cm^{-3}$. This is much lower than the reported values (~$2 \times 10^7$ molecules $cm^{-3}$) for airborne observations over the boundary layer of Northeastern U.S. and the Ohio Valley region during NEAQS-2004.[40,41] As one of the major aims of the NEAQS-2004 campaign was to sample power plant plumes, it is


DOI: 10.1021/es505793t
Environ. Sci. Technol. 2015, 49, 3383−3391

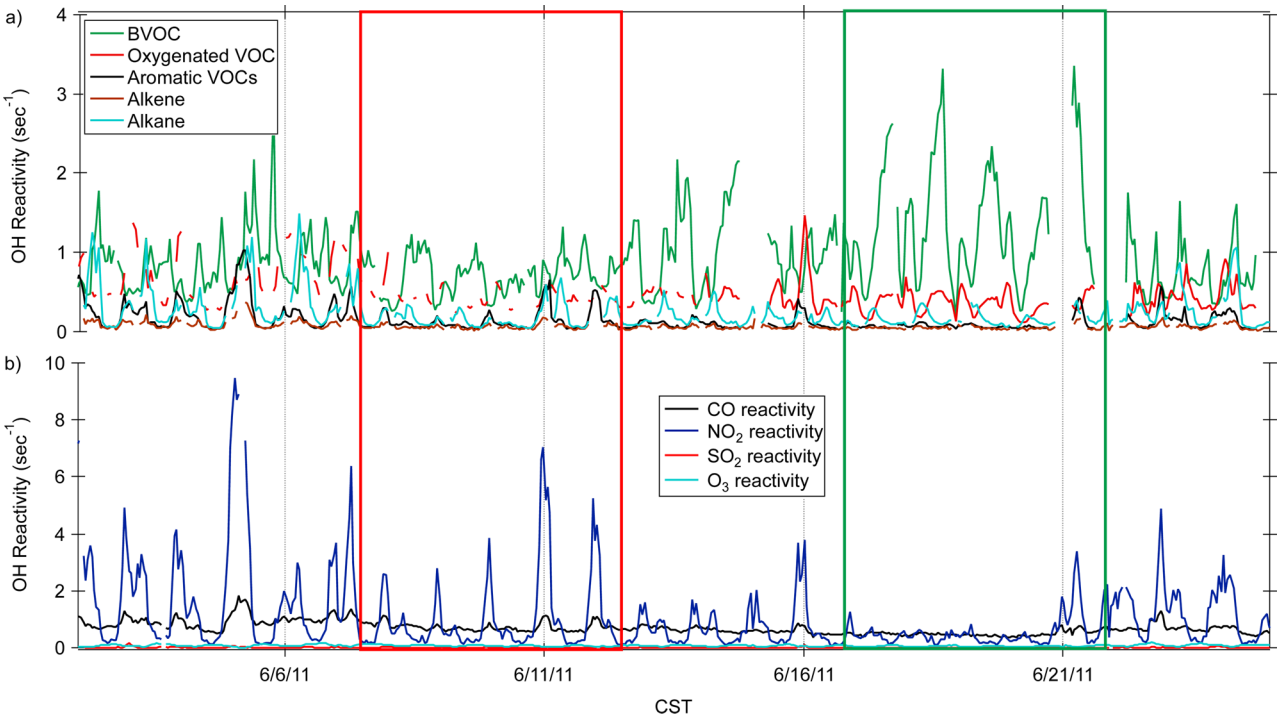


**Figure 1.** Calculated OH reactivity ($s^{-1}$, a multiplication of the concentration of a gas species and its reaction rate constant with OH) from different observed (a) VOC classes and (b) criteria trace gases. The average daytime (11:00 to 17:00) OH reactivity for the sums of the presented chemical classes are 2.4 $s^{-1}$ and 3.4 $s^{-1}$ for the low BVOC (the red rectangle) and the high BVOC (the green rectangle) periods, respectively. Alkane: ethane, propane, isobutene, *n*-butane, cyclopentane, isopentane, *n*-pentane, *n*-hexane, heptane; alkene: ethene, 1-butene, 1,3-butadiene, *t*2-pentene; OVOCs: acetone, hydroxyacetone, methylglyoxal, methyl ethyl ketone; BVOCs: isoprene, monoterpenes, methyl vinyl ketone+methacrolein; and aromatics: benzene, toluene, C8-aromatics, C9-aromatics.

understandable that the observed $H_2SO_4$ levels from NEAQS-2004 are higher than those from this study. However, limited previous observations indicate that local pollution levels are not necessarily directly correlated with observed $H_2SO_4$. For example, the observed averaged daytime maxima of $H_2SO_4$ from Mexico City, Mexico[40] and Beijing, China[42] were reported as $1.6 \times 10^7$ and $5 \times 10^6$ molecules $cm^{-3}$, respectively, although the observed $SO_2$ levels were at similar levels of ~5−10 ppb for both campaigns. This nonlinearity between $H_2SO_4$ and its precursor, $SO_2$, suggests that better understanding of the $H_2SO_4$ source and sink relationship is needed to accurately predict the atmospheric distributions of $H_2SO_4$.[43]

The model calculated sCI concentrations presented in Figure 3 include the total sCI number densities and the speciated sCI number densities. For comparative purposes, we conducted the identical calculations for a time period with decreased BVOC influence, indicated by the red rectangle in Figure 1. As shown in Figure 3a, the total sCIs during the period of decreased BVOCs are assessed to be approximately half of the total sCIs during the high BVOC period in the afternoon. Therefore, the discussion is focused on the high BVOC period henceforth. Among the calculated sCI species, sCI from $\alpha$-pinene (APINBOO), isoprene (MVKOO and MACROO), and $\beta$-pinene (NOPINOO) ozonolysis compose most of total sCIs, along with $CH_2OO$ (Figure 3b). Overall, the calculated peak sCI levels are higher than the maximum sCI levels (~$1 \times 10^4$ molecules $cm^{-3}$) predicted by a regional model for the summer season.[21] It should be noted that the direct comparison between the short-term observationally based estimation and the seasonal estimate of the regional model (12-km resolution) should be cautiously interpreted.

Theses outcomes are calculated using default MCM 3.2 rate constants, which apply $k_{R5a}$ and $k_{R5b}$ as $5.0 \times 10^{-18}$ and $1.0 \times 10^{-17}$ molecules$^{-1}$ $cm^3$ $s^{-1}$, respectively. Recent studies have also highlighted the uncertainty in the rate constant of R5 (R5a + R5b) as the reaction with water vapor mostly determines the chemical loss rates of sCIs. The published range of the rate constant for R5[35] is $2 \times 10^{-19}$ to $1 \times 10^{-15}$ molecules $cm^3$ $s^{-1}$. A series of more recent laboratory and theoretical studies also presented a wide range of recommendations for the reaction rates of $R_5$. Welz et al.[12,44] reported a significantly higher upper limit for $k_{R5}$ ($k_{R5a+R5b} = 4 \times 10^{-15}$ molecules $cm^3$ $s^{-1}$) compared to the $9 \times 10^{-17}$ molecules $cm^3$ $s^{-1}$ from Stone et al.[13] Stone et al.[13] also experimentally derived $k_{R5a}$ ($5.4 \times 10^{-17}$ molecules $cm^3$ $s^{-1}$), very close to that applied in MCM 3.2. Theoretical studies[45,46] evaluating the kinetics of sCI with water dimer argue that a reaction with water dimer becomes the dominant sCI chemical sink especially for the small sCI. Verecken et al.[46] presented zero-dimensional model simulation results indicating that $CH_2OO$ mostly (99 to 100%) reacts with water dimer under typical boundary layer conditions ranging from boreal forest to mega city environments. Therefore, if we include the fast water dimer reaction in the zero-dimensional model calculation, it results in no contribution to $H_2SO_4$ formation from R4. For comparison purpose, we calculated $CH_2OO$ with the upper limit of $k_{R5}$ presented by Welz et al.[12] The results shown in Figure 3c suggest significant suppression in $CH_2OO$ by applying the fast $k_{R5}$, which would cause substantially less contribution of the sCI reaction channel to $H_2SO_4$ formation. Further studies on chemical interactions between water vapor and sCIs are urged in this context.





DOI: 10.1021/es505793t
*Environ. Sci. Technol.* 2015, 49, 3383−3391

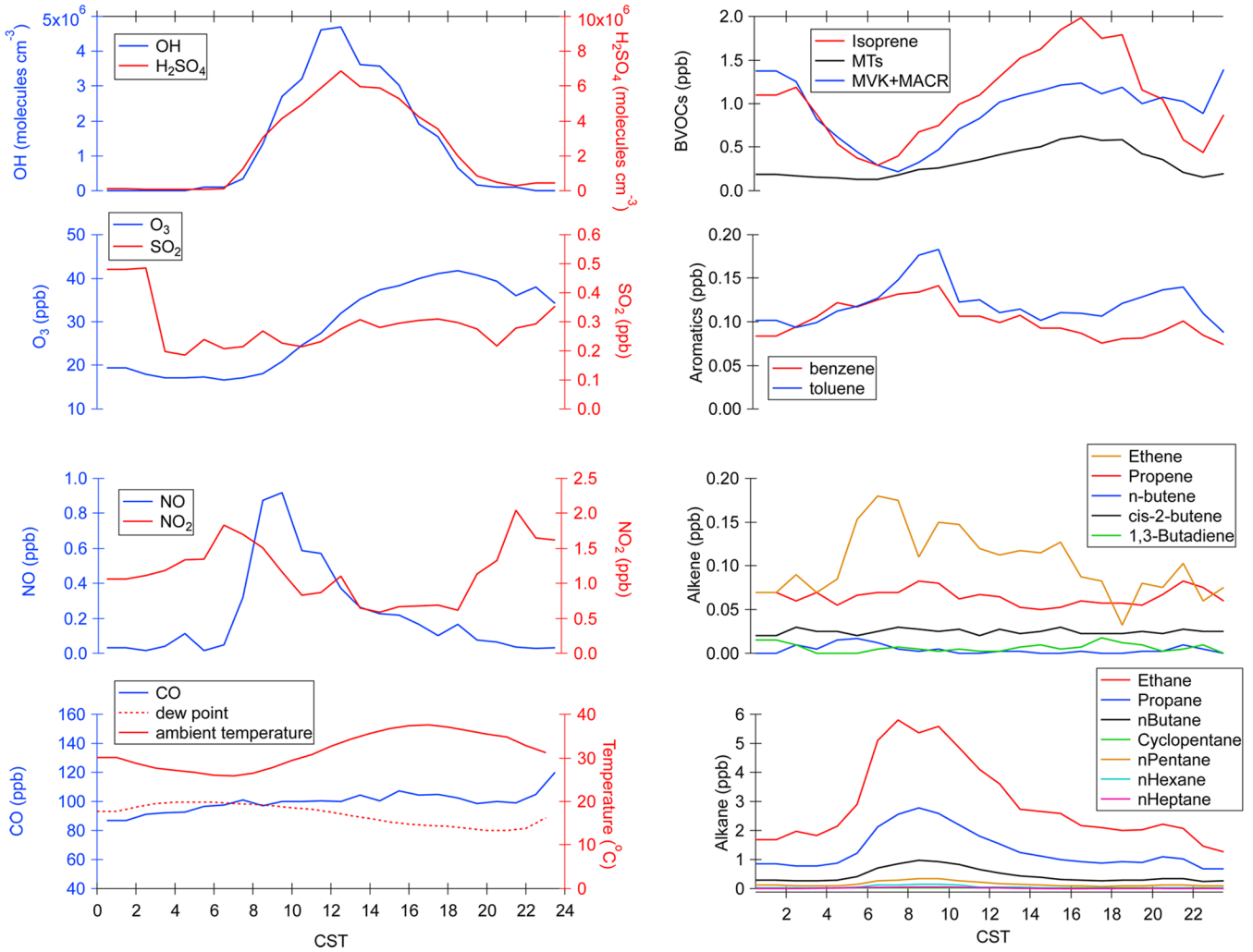


**Figure 2.** Average diurnal profiles (June 17th to June 21st) of observed gas species, ambient temperature and *dew points during DFW-2011. These observations are used to constrain the zero-dimensional model when calculating sCI concentrations. MTs represent monoterpenes, and MVK+MACR is the sum of the isoprene oxidation products methyl-vinyl-ketone and methacrolein. *In the relative humidity scale, the diurnal variation is ranging from ~25% to ~75%.

Considering the reaction rate constant for R1 is $1.3 \times 10^{-12}$ $cm^3$ $s^{-1}$ when expressed as second order at 298 K and 1 atm, sCI is not likely to make significant contributions to $H_2SO_4$ production compared to OH, especially in the morning to noon. The peak of total sCI concentrations was observed in the late afternoon, coinciding with the afternoon $O_3$ enhancement shown in Figure 2. As reviewed above, the rate constants of $SO_2$ with $CH_2OO$[12] ($k_{Welz}$) and monoterpene sCIs[15] ($k_{Mauldin}$) have been experimentally determined and are significantly different ($k_{Welz}/k_{Mauldin}$ = 65). Empirical rate constants of sCIs from isoprene ozonolysis and $SO_2$ have not been reported, as only relative rate coefficients are available.[16] Therefore, there is significant uncertainty in $H_2SO_4$ production rate estimations depending upon which reaction rate constant is applied. To examine this uncertainty, the $H_2SO_4$ production rates were calculated by applying two different estimates of reaction rate constants, as summarized in Table 2. Scenario I applied $k_{Welz}$ for reactions of $SO_2$ with sCIs to estimate the maximum $H_2SO_4$ forming potential from the sCI reaction channel. However, Scenario II constrains the low end of contributions of the sCI reaction channel to the $H_2SO_4$ production by applying $k_{Mauldin}$ to the sCI reactions with $SO_2$. $H_2SO_4$ formation rates from the sCI (Figure 3b) and OH reaction channels are compared in Figure 4.

In the bottom panel, the diurnal variations of $H_2SO_4$ formation rates from $SO_2$ + OH (in red) and sCI + $SO_2$ (in blue) are presented. On the top panel, the ratios of $H_2SO_4$ production rates from the sCI reaction channel to the OH reaction channel are presented. As expected, the relative importance of the sCI reaction channel becomes more significant in the afternoon, but the magnitude depends on the scenario. For example, at noon, the $H_2SO_4$ production rate ratio, presented in the upper panel of Figure 4, is estimated to be ~15% for Scenario I. In contrast, only ~0.2% is estimated for Scenario II. In addition, the sCI reaction channel is the only apparent $H_2SO_4$ production pathway during the night when observed OH was below the detection limit. Nighttime $H_2SO_4$ production rate estimates vary over a wide range due to the different reaction constants applied in different calculation scenarios. This uncertainty needs to be addressed, as the cause of nighttime new particle formation events continues to puzzle the scientific community.[47] It is known that new particle formation events are mostly driven by the significant presence of $H_2SO_4$[4]. Because the importance of sCI as an oxidant for $SO_2$ has been underestimated, the prevailing hypothesis has been the





DOI: 10.1021/es505793t
Environ. Sci. Technol. 2015, 49, 3383−3391

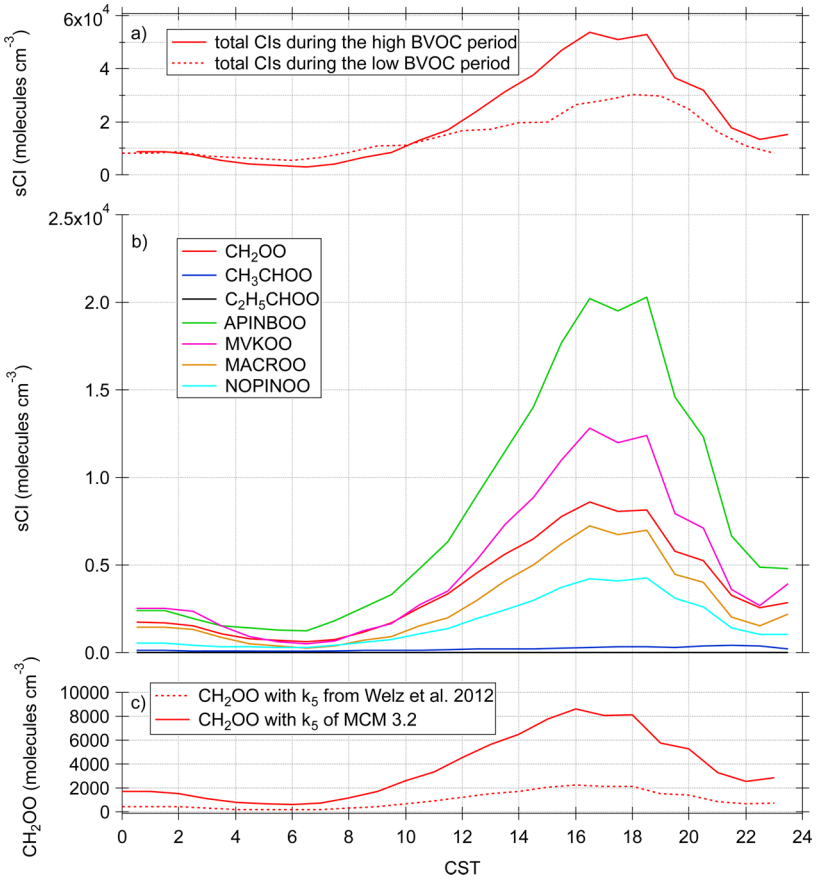


**Figure 3.** UWCM zero-dimensional model calculations of (a) the diurnal variation of total sCI concentrations, (b) the diurnal variations of speciated sCI concentrations during the high BVOC period, and (c) the comparison of $CH_2OO$ concentrations by applying two different $k_5$ in the model. The model outcomes with Scenario II (Table 2) are shown.

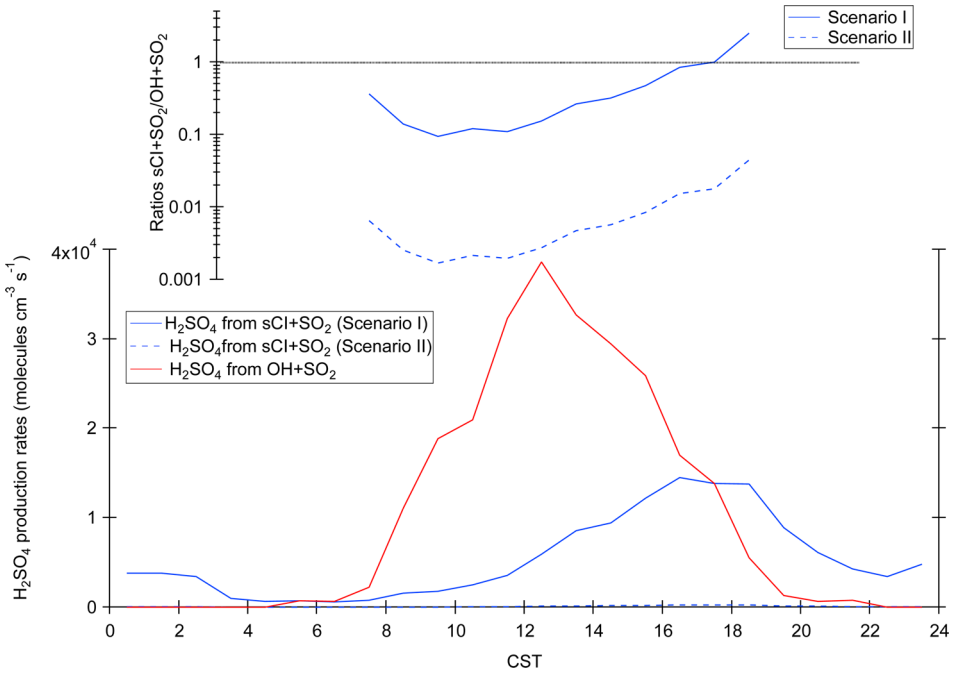


**Figure 4.** Comparison between OH (red) and sCI (blue) oxidation channels (bottom panel). Two different sCI + $SO_2$ scenarios are compared by applying two different rate constants for isoprene sCIs indicated by dashed and solid blue lines. The ratios of $H_2SO_4$ production rates between the sCI and the OH production channels are shown in the top panel. The systematic differences between Scenario I and Scenario II are caused by the applications of different rate constants for sCIs from isoprene ozonloysis, as shown in Table 2.





DOI: 10.1021/es505793t
*Environ. Sci. Technol.* 2015, 49, 3383−3391

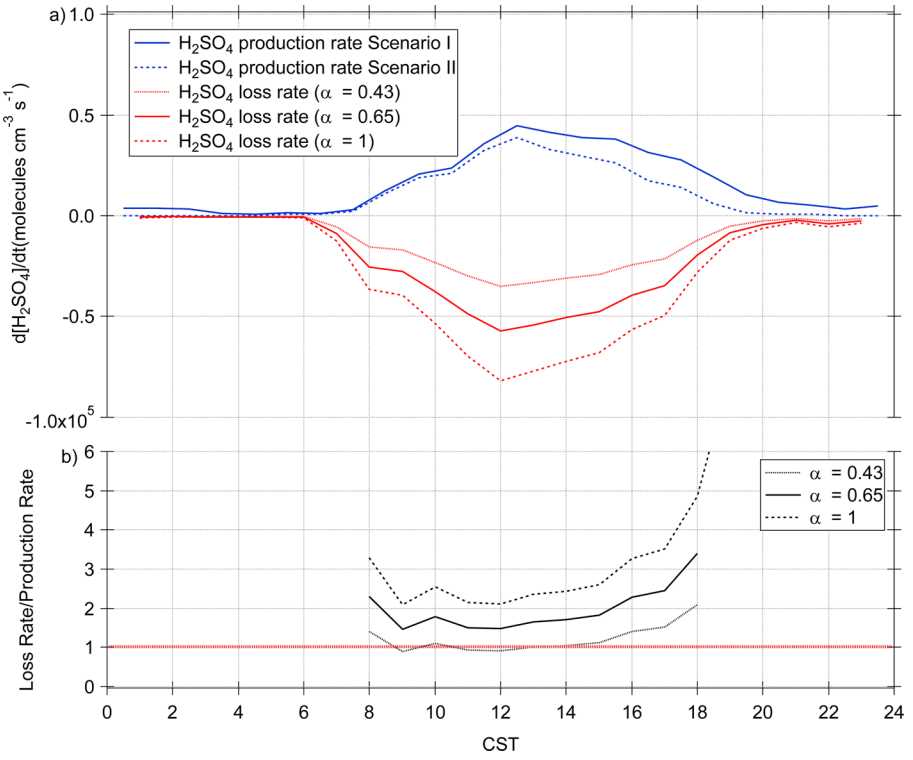


**Figure 5.** (a) The diurnal variations of calculated $H_2SO_4$ production (blue) and loss rates (red). Three different loss rate calculations with different mass accommodation coefficients ($\alpha$) are presented and two different production rate calculations with the different combinations of production channels and reaction constants are presented. (b) The ratios of loss to production rates of $H_2SO_4$. The production rates from the model calculation Scenario II with loss rates calculated using different $\alpha$ values are presented.

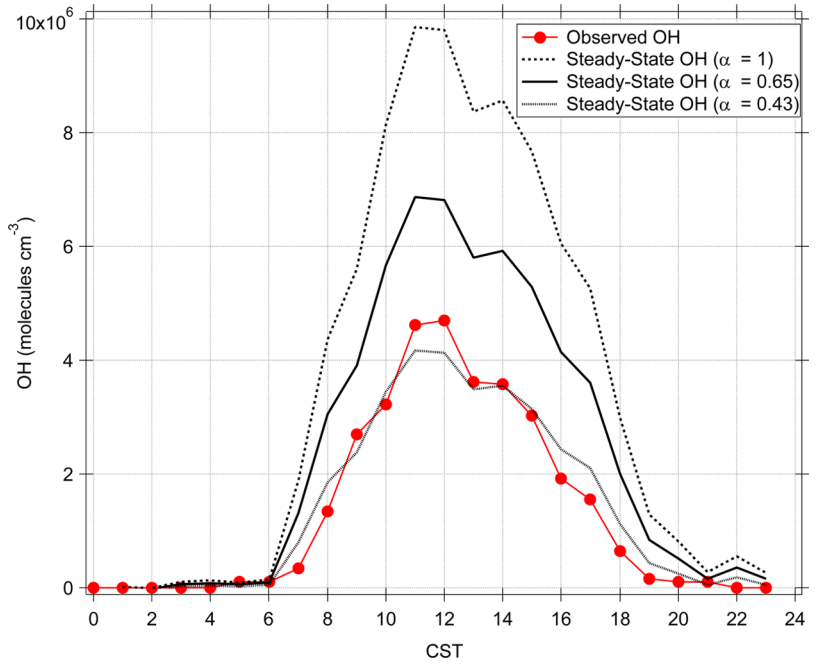


**Figure 6.** Diurnal variations of $[OH]_{SS}$ (eq 3) and $[OH]_{Observed}$.

existence of nighttime OH to trigger R1. However, we did not observe detectable levels of nighttime OH in this study.

Finally, we calculate the loss rates of $H_2SO_4$ to compare with the estimated $H_2SO_4$ production rates. Using measured aerosol surface area, $H_2SO_4$ loss rates from diffusion-limited $H_2SO_4$ aerosol uptake (molecules $s^{-1}$) are estimated as follows:

$$R_{AU} = (4/(\alpha\upsilon))^{-1} A n_x \quad (1)$$

where AU is the aerosol uptake, $\alpha$ is the mass accommodation coefficient, $\upsilon$ is the molecular speed (cm $s^{-1}$), $A$ is the Fuchs surface area ($cm^2$), and $n_x$ is the concentration of $H_2SO_4$ (molecules $cm^{-3}$). As $\upsilon$ (through temperature and pressure), $A$, and $n_x$ are constrained observationally, the main uncertainty of





DOI: 10.1021/es505793t
Environ. Sci. Technol. 2015, 49, 3383−3391

the estimation is associated with $\alpha$. Previous studies[40,41,48] have consistently applied a value of 0.65 that was recommended by a laboratory flow tube study,[49] with a lower limit of 0.43 and an upper limit of 1. Calculated $H_2SO_4$ aerosol uptake rates using the recommended, upper, and lower values are shown as red traces in Figure 5. In addition, the diurnal profiles of $H_2SO_4$ production rates are shown in blue. A number of studies[40,41] have deduced OH concentrations by assuming pseudo steady-state for $H_2SO_4$ (loss rate = formation rate) and solving for OH:

$$(4/(\alpha v))^{-1} A n_x = k_{R1}[OH][SO_2] + k_{R4}[sCI][SO_2] \quad (2)$$

$$[OH]_{SS} = \frac{\left(\frac{4}{\alpha v}\right)^{-1} A n_x - k_{R4}[sCI][SO_2]}{k_{R1}[SO_2]} \quad (3)$$

The comparisons between production and loss rates in Figure 5a indicate that the $H_2SO_4$ production rates from all calculation scenarios are substantially lower than $H_2SO_4$ loss rates calculated with an accommodation rate of 0.65. The application of the lower limit (0.43) in the $H_2SO_4$ loss rate calculation results in a good agreement between the $H_2SO_4$ loss and the production rates. More quantitative comparisons are presented in Figure 5b, showing the ratios of $H_2SO_4$ loss to production rates. In this analysis, we applied Scenario II for the sCI contribution to $H_2SO_4$ production to compare with the previous studies,[40,41] considering a minimal sCI contribution to $H_2SO_4$ production. When the lower limit ($\alpha$ = 0.43) was applied, the ratios were calculated mostly close to 1, as the higher mass accommodation coefficients cause substantial overestimation of $H_2SO_4$ loss rates. The ratios are 1.44 and 2.05 at noon for $\alpha$ = 0.65 and $\alpha$ = 1.0, respectively.

The DFW area was under very hot and dry conditions during the observational period as shown in Figure 2. Therefore, it may not be appropriate to apply the empirical mass accommodation coefficient deduced from the experimental setup of $H_2SO_4$ uptake. This systematic overestimation of $H_2SO_4$ loss rates would cause overestimation of OH using the pseudo steady-state equation as shown in Figure 6. The figure clearly shows that the application of the recommended mass accommodation coefficient causes significant overestimation of steady-state OH ($[OH]_{SS}$) with respect to the observed OH diurnal variations. The lower limit of the mass accommodation coefficient (0.43) results in a diurnal variation of $[OH]_{SS}$ in agreement with the observed [OH] diurnal variation. Indeed, the calculation scheme using a data set from Mexico City, another very dry environment, indicate the substantial systematic overestimation (~30%) of observed OH concentrations, which is consistent with our analysis results.[40]

## AUTHOR INFORMATION


### Corresponding Author

*Phone:1-949-824-4531; fax: 1-949-824-3874; e-mail:saewungk@uci.edu (S.K.).


### Notes

The authors declare no competing financial interest.

## ACKNOWLEDGMENTS

This study was supported by the TCEQ Air Quality Research Program. Support of A. P. Rutter by the Dreyfus Foundation is gratefully acknowledged. The authors would like to thank Melanie Calzada and Caroline Gutierrez for their help in data collection in the field and the Texas National Guard for providing access to the Eagle Mountain Lake site.

## REFERENCES


(1) Tyndall, G. S.; Ravishankara, A. R. Atmospheric oxidation of reduced sulfur species. *Int. J. Chem. Kinet.* **1991**, *23* (6), 483−527.

(2) Calvert, J. G.; Stockwell, W. R. Acid generation in the troposphere by gas-phase chemistry. *Environ. Sci. Technol.* **1983**, *17* (9), A428−A443.

(3) Ramanathan, V.; Crutzen, P. J.; Kiehl, J. T.; Rosenfeld, D. Atmosphere—Aerosols, climate, and the hydrological cycle. *Science* **2001**, *294* (5549), 2119−2124.

(4) Sipila, M.; Berndt, T.; Petaja, T.; Brus, D.; Vanhanen, J.; Stratmann, F.; Patokoski, J.; Mauldin, R. L.; Hyvarinen, A. P.; Lihavainen, H.; Kulmala, M. The role of sulfuric acid in atmospheric nucleation. *Science* **2010**, *327* (5970), 1243−1246.

(5) Berndt, T.; Boge, O.; Stratmann, F.; Heintzenberg, J.; Kulmala, M. Rapid formation of sulfuric acid particles at near-atmospheric conditions. *Science* **2005**, *307* (5710), 698−700.

(6) Seinfeld, J. H.; Pandis, S. N. *Atmospheric Chemistry and Physics-From Air Pollution to Climate Change*, Second ed.; John Wiley & Sons, Inc.: New York, 2006; p 1202.

(7) Calvert, J. G.; Su, F.; Bottenheim, J. W.; Strausz, O. P. Mechanism of homogeneous oxidation of sulfur-dioxide in troposphere. *Atmos. Environ.* **1978**, *12* (1−3), 197−226.

(8) Criegee, R. Mechanism of ozonolysis. *Angew. Chem. Int. Edit* **1975**, *14* (11), 745−752.

(9) Cox, R. A.; Penkett, S. A. Oxidation of atmospheric $SO_2$ by products of ozone−olefin reaction. *Nature* **1971**, *230* (5292), 321−322.

(10) Hatakeyama, S.; Kobayashi, H.; Akimoto, H. Gas-phase oxidation of $SO_2$ in the ozone olefin reactions. *J. Phys. Chem.* **1984**, *88* (20), 4736−4739.

(11) Johnson, D.; Lewin, A. G.; Marston, G. The effect of Criegee-intermediate scavengers on the OH yield from the reaction of ozone with 2-methylbut-2-ene. *J. Phys. Chem. A* **2001**, *105* (13), 2933−2935.

(12) Welz, O.; Savee, J. D.; Osborn, D. L.; Vasu, S. S.; Percival, C. J.; Shallcross, D. E.; Taatjes, C. A. Direct kinetic measurements of Criegee intermediate ($CH_2OO$) formed by reaction of $CH_2I$ with $O_2$. *Science* **2012**, *335* (6065), 204−207.

(13) Stone, D.; Blitz, M.; Daubney, L.; Howes, N. U. M.; Seakins, P. Kinetics of $CH_2OO$ reactions with $SO_2$, $NO_2$, NO, $H_2O$ and $CH_3CHO$ as a function of pressure. *Phys. Chem. Chem. Phys.* **2014**, *16* (3), 1139−1149.

(14) Taatjes, C. A.; Welz, O.; Eskola, A. J.; Savee, J. D.; Scheer, A. M.; Shallcross, D. E.; Rotavera, B.; Lee, E. P. F.; Dyke, J. M.; Mok, D. K. W.; Osborn, D. L.; Percival, C. J. Direct measurements of conformer-dependent reactivity of the Criegee intermediate $CH_3CHOO$. *Science* **2013**, *340* (6129), 177−180.

(15) Mauldin, R. L.; Berndt, T.; Sipila, M.; Paasonen, P.; Petaja, T.; Kim, S.; Kurten, T.; Stratmann, F.; Kerminen, V. M.; Kulmala, M. A new atmospherically relevant oxidant of sulphur dioxide. *Nature* **2012**, *488* (7410), 193−197.

(16) Sipila, M.; Jokinen, T.; Berndt, T.; Richters, S.; Makkonen, R.; Donahue, N. M.; Mauldin, R. L.; Kurten, T.; Paasonen, P.; Sarnela, N.; Ehn, M.; Junninen, H.; Rissanen, M. P.; Thornton, J.; Stratmann, F.; Herrmann, H.; Worsnop, D. R.; Kulmala, M.; Kerminen, V. M.; Petaja, T. Reactivity of stabilized Criegee intermediates (sCIs) from isoprene and monoterpene ozonolysis toward $SO_2$ and organic acids. *Atmos Chem. Phys.* **2014**, *14* (22), 12143−12153.

(17) Carlsson, P. T. M.; Keunecke, C.; Kruger, B. C.; Maass, M. C.; Zeuch, T. Sulfur dioxide oxidation induced mechanistic branching and particle formation during the ozonolysis of beta-pinene and 2-butene. *Phys. Chem. Chem. Phys.* **2012**, *14* (45), 15637−15640.

(18) Boy, M.; Mogensen, D.; Smolander, S.; Zhou, L.; Nieminen, T.; Paasonen, P.; Plass-Dulmer, C.; Sipila, M.; Petaja, T.; Mauldin, L.; Berresheim, H.; Kulmala, M. Oxidation of $SO_2$ by stabilized Criegee intermediate (sCI) radicals as a crucial source for atmospheric sulfuric acid concentrations. *Atmos Chem. Phys.* **2013**, *13* (7), 3865−3879.

(19) Pierce, J. R.; Evans, M. J.; Scott, C. E.; D'Andrea, S. D.; Farmer, D. K.; Swietlicki, E.; Spracklen, D. V. Weak global sensitivity of cloud






DOI: 10.1021/es505793t
*Environ. Sci. Technol.* 2015, 49, 3383−3391

condensation nuclei and the aerosol indirect effect to Criegee + $SO_2$ chemistry. *Atmos Chem. Phys.* **2013**, *13* (6), 3163−3176.
(20) Li, J. Y.; Ying, Q.; Yi, B. Q.; Yang, P. Role of stabilized Criegee Intermediates in the formation of atmospheric sulfate in eastern United States. *Atmos. Environ.* **2013**, *79*, 442−447.
(21) Sarwar, G.; Simon, H.; Fahey, K.; Mathur, R.; Goliff, W. S.; Stockwell, W. R. Impact of sulfur dioxide oxidation by stabilized Criegee intermediate on sulfate. *Atmos. Environ.* **2014**, *85*, 204−214.
(22) Weber, R. J.; McMurry, P. H.; Mauldin, R. L.; Tanner, D. J.; Eisele, F. L.; Clarke, A. D.; Kapustin, V. N. New particle formation in the remote troposphere: A comparison of observations at various sites. *Geophys. Res. Lett.* **1999**, *26* (3), 307−310.
(23) Graus, M.; Muller, M.; Hansel, A. High resolution PTR-TOF: Quantification and formula confirmation of VOC in real time. *J. Am. Soc. Mass Spectrom.* **2010**, *21* (6), 1037−1044.
(24) Blake, R. S.; Monks, P. S.; Ellis, A. M. Proton-transfer reaction mass spectrometry. *Chem. Rev.* **2009**, *109* (3), 861−896.
(25) Muller, M.; Graus, M.; Ruuskanen, T. M.; Schnitzhofer, R.; Bamberger, I.; Kaser, L.; Titzmann, T.; Hortnagl, L.; Wohlfahrt, G.; Karl, T.; Hansel, A. First eddy covariance flux measurements by PTR-TOF. *Atmos. Meas. Tech.* **2010**, *3* (2), 387−395.
(26) Kaser, L.; Karl, T.; Schnitzhofer, R.; Graus, M.; Herdlinger-Blatt, I. S.; DiGangi, J. P.; Sive, B.; Turnipseed, A.; Hornbrook, R. S.; Zheng, W.; Flocke, F. M.; Guenther, A.; Keutsch, F. N.; Apel, E.; Hansel, A. Comparison of different real time VOC measurement techniques in a ponderosa pine forest. *Atmos. Chem. Phys.* **2013**, *13* (5), 2893−2906.
(27) Tanner, D. J.; Jefferson, A.; Eisele, F. L. Selected ion chemical ionization mass spectrometric measurement of OH. *J. Geophys. Res.* **1997**, *102* (D5), 6415−6425.
(28) Kim, S.; VandenBoer, T. C.; Young, C. J.; Riedel, T. P.; Thornton, J. A.; Swarthout, B.; Sive, B.; Lerner, B.; Gilman, J. B.; Warneke, C.; Roberts, J. M.; Guenther, A.; Wagner, N. L.; Dube, W. P.; Williams, E.; Brown, S. S. The primary and recycling sources of OH during the NACHTT-2011 campaign: HONO as an important OH primary source in the wintertime. *J. Geophys. Res.-Atmos.* **2014**, *119* (11), 6886−6896.
(29) Kim, S.; Wolfe, G. M.; Mauldin, L.; Cantrell, C.; Guenther, A.; Karl, T.; Turnipseed, A.; Greenberg, J.; Hall, S. R.; Ullmann, K.; Apel, E.; Hornbrook, R.; Kajii, Y.; Nakashima, Y.; Keutsch, F. N.; DiGangi, J. P.; Henry, S. B.; Kaser, L.; Schnitzhofer, R.; Graus, M.; Hansel, A.; Zheng, W.; Flocke, F. F. Evaluation of $HO_x$ sources and cycling using measurement-constrained model calculations in a 2-methyl-3-butene-2-ol (MBO) and monoterpene (MT) dominated ecosystem. *Atmos Chem. Phys.* **2013**, *13* (4), 2031−2044.
(30) Wolfe, G. M.; Thornton, J. A. The chemistry of atmosphere-forest exchange (CAFE) model—Part 1: Model description and characterization. *Atmos. Chem. Phys.* **2011**, *11* (1), 77−101.
(31) Jenkin, M. E.; Saunders, S. M.; Pilling, M. J. The tropospheric degradation of volatile organic compounds: A protocol for mechanism development. *Atmos. Environ.* **1997**, *31* (1), 81−104.
(32) Jenkin, M. E.; Saunders, S. M.; Wagner, V.; Pilling, M. J. Protocol for the development of the Master Chemical Mechanism, MCM v3 (Part B): Tropospheric degradation of aromatic volatile organic compounds. *Atmos. Chem. Phys.* **2003**, *3*, 181−193.
(33) Saunders, S. M.; Jenkin, M. E.; Derwent, R. G.; Pilling, M. J. Protocol for the development of the Master Chemical Mechanism, MCM v3 (Part A): Tropospheric degradation of non-aromatic volatile organic compounds. *Atmos. Chem. Phys.* **2003**, *3*, 161−180.
(34) Archibald, A. T.; Cooke, M. C.; Utembe, S. R.; Shallcross, D. E.; Derwent, R. G.; Jenkin, M. E. Impacts of mechanistic changes on $HO_x$ formation and recycling in the oxidation of isoprene. *Atmos. Chem. Phys.* **2010**, *10* (17), 8097−8118.
(35) Hatakeyama, S.; Akimoto, H. Reactions of Criegee intermediates in the gas-phase. *Res. Chem. Intermed.* **1994**, *20* (3−5), 503−524.
(36) Kim, S.; Kim, S.-Y.; Lee, M.; Shim, H.; Wolfe, G. M.; Guenther, A. B.; He, A.; Hong, Y.; Han, J. Urban-rural interactions in a South Korea forest: Uncertainties in isoprene−OH intereactions limit our understanding of ozone and secondary organic aerosol production. *Atmos. Chem. Phys. Discuss.* **2014**, *14*, 16691−16729.
(37) Mao, J.; Ren, X.; Zhang, L.; Van Duin, D. M.; Cohen, R. C.; Park, J. H.; Goldstein, A. H.; Paulot, F.; Beaver, M. R.; Crounse, J. D.; Wennberg, P. O.; DiGangi, J. P.; Henry, S. B.; Keutsch, F. N.; Park, C.; Schade, G. W.; Wolfe, G. M.; Thornton, J. A.; Brune, W. H. Insights into hydroxyl measurements and atmospheric oxidation in a California forest. *Atmos Chem. Phys.* **2012**, *12* (17), 8009−8020.
(38) Mao, J. Q.; Ren, X. R.; Chen, S. A.; Brune, W. H.; Chen, Z.; Martinez, M.; Harder, H.; Lefer, B.; Rappengluck, B.; Flynn, J.; Leuchner, M. Atmospheric oxidation capacity in the summer of Houston 2006: Comparison with summer measurements in other metropolitan studies. *Atmos. Environ.* **2010**, *44* (33), 4107−4115.
(39) Stone, D.; Whalley, L. K.; Heard, D. E. Tropospheric OH and $HO_2$ radicals: Field measurements and model comparisons. *Chem. Soc. Rev.* **2012**, *41* (19), 6348−6404.
(40) Case-Hanks, A. T. *Formaldehyde Isntrument Development and Boundary Layer Sulfuric Acid: Implications for Photochemistry*; Georgia Institute of Technology: Atlanta, GA, 2008.
(41) Warneke, C.; de Gouw, J. A.; Del Negro, L.; Brioude, J.; McKeen, S.; Stark, H.; Kuster, W. C.; Goldan, P. D.; Trainer, M.; Fehsenfeld, F. C.; Wiedinmyer, C.; Guenther, A. B.; Hansel, A.; Wisthaler, A.; Atlas, E.; Holloway, J. S.; Ryerson, T. B.; Peischl, J.; Huey, L. G.; Hanks, A. T. C. Biogenic emission measurement and inventories determination of biogenic emissions in the eastern United States and Texas and comparison with biogenic emission inventories. *J. Geophys. Res.-Atmos.* **2010**, *115*.
(42) Zheng, J.; Hu, M.; Zhang, R.; Yue, D.; Wang, Z.; Guo, S.; Li, X.; Bohn, B.; Shao, M.; He, L.; Huang, X.; Wiedensohler, A.; Zhu, T. Measurements of gaseous $H_2SO_4$ by AP-ID-CIMS during CAREBeijing 2008 Campaign. *Atmos. Chem. Phys.* **2011**, *11* (15), 7755−7765.
(43) Mikkonen, S.; Romakkaniemi, S.; Smith, J. N.; Korhonen, H.; Petaja, T.; Plass-Duelmer, C.; Boy, M.; McMurry, P. H.; Lehtinen, K. E. J.; Joutsensaari, J.; Hamed, A.; Mauldin, R. L.; Birmili, W.; Spindler, G.; Arnold, F.; Kulmala, M.; Laaksonen, A. A statistical proxy for sulphuric acid concentration. *Atmos. Chem. Phys.* **2011**, *11* (21), 11319−11334.
(44) Welz, O.; Eskola, A. J.; Sheps, L.; Rotavera, B.; Savee, J. D.; Scheer, A. M.; Osborn, D. L.; Lowe, D.; Booth, A. M.; Xiao, P.; Khan, M. A. H.; Percival, C. J.; Shallcross, D. E.; Taatjes, C. A. Rate coefficients of C1 and C2 Criegee intermediate reactions with formic and acetic acid near the collision limit: Direct kinetics measurements and atmospheric implications. *Angew. Chem. Int. Ed.* **2014**, *53* (18), 4547−4550.
(45) Ryzhkov, A. B.; Ariya, P. A. A theoretical study of the reactions of parent and substituted Criegee intermediates with water and the water dimer. *Phys. Chem. Chem. Phys.* **2004**, *6* (21), 5042−5050.
(46) Vereecken, L.; Harder, H.; Novelli, A. The reactions of Criegee intermediates with alkenes, ozone, and carbonyl oxides. *Phys. Chem. Chem. Phys.* **2014**, *16* (9), 4039−4049.
(47) Lee, S. H.; Young, L. H.; Benson, D. R.; Suni, T.; Kulmala, M.; Junninen, H.; Campos, T. L.; Rogers, D. C.; Jensen, J. Observations of nighttime new particle formation in the troposphere. *J. Geophys. Res.: Atmos.* **2008**, *113* (D10).
(48) Chen, G.; Huey, L. G.; Trainer, M.; Nicks, D.; Corbett, J.; Ryerson, T.; Parrish, D.; Neuman, J. A.; Nowak, J.; Tanner, D.; Holloway, J.; Brock, C.; Crawford, J.; Olson, J. R.; Sullivan, A.; Weber, R.; Schauffler, S.; Donnelly, S.; Atlas, E.; Roberts, J.; Flocke, F.; Hubler, G.; Fehsenfeld, F. An investigation of the chemistry of ship emission plumes during ITCT 2002. *J. Geophys. Res.: Atmos.* **2005**, *110* (D10).
(49) Poschl, U.; Canagaratna, M.; Jayne, J. T.; Molina, L. T.; Worsnop, D. R.; Kolb, C. E.; Molina, M. J. Mass accommodation coefficient of $H_2SO_4$ vapor on aqueous sulfuric acid surfaces and gaseous diffusion coefficient of $H_2SO_4$ in $N_2/H_2O$. *J. Phys. Chem. A* **1998**, *102* (49), 10082−10089.


DOI: 10.1021/es505793t
*Environ. Sci. Technol.* 2015, 49, 3383−3391